Supporting Information for

High-Performance Flexible Energy Storage Device from Biomass-Derived Porous Carbon Supported MnCo$_2$O$_4$ Nanorods and MnO$_2$ Nanoscales

Debika Gogoi,[a] Rajeshvari Samatbhai Karmur,[a] Manash R. Das,[b,c] Narendra Nath Ghosh*[a]

[a] Nano-materials Lab, Department of Chemistry, Birla Institute of Technology and Science, Pilani K K Birla Goa Campus, Zuarinagar 403726, Goa, India.

[b] Advanced Materials Group, Materials Sciences and Technology Division, CSIR-North East Institute of Science and Technology, Jorhat 785006, Assam, India.

[c] Academy of Scientific and Innovative Research (AcSIR), Ghaziabad 201002, India.

*Corresponding author. Tel. /fax: +91 832 2580318/25570339.
*E-mail address: naren70@yahoo.com (N. N. Ghosh)
Author's email addresses: p20180429@goa.bits-pilani.ac.in (Debika Gogoi),
p20200051@goa.bits-pilani.ac.in (Rajeshvari Samatbhai Karmur)
mnshrdas@yahoo.com (Manash R. Das)

S1. Materials and Methods

S1.1. Chemicals used. Cobalt chloride hexahydrate ($CoCl_2.6H_2O$) and Manganese chloride tetrahydrate ($MnCl_2.4H_2O$), were purchased from Merck, India. Potassium Permanganate ($KMnO_4$), Sulphuric acid (H_2SO_4), Potassium Hydroxide (KOH), Potassium Ferrocyanide ($K_4[Fe(CN)6]$, and ethanol were purchased from Fisher Scientific. Polyvinylidene difluoride (PVDF), acetylene black, N-methyl-2-pyrrolidinone (NMP), and polyvinyl alcohol (PVA) were purchased from Sigma-Aldrich. All the chemicals were used without further purification. Deionized water was used throughout the experiment.

S1.2. Synthesis of MnCo$_2$O$_4$

An aqueous solution of $MnCl_2.4H_2O$ and $CoCl_2.6H_2O$ (1:2 mole ratio) were mixed in a beaker and 12 moles of urea solution was added to it and then the reaction mixture was allowed to stir for 30 min at room temperature. After that, the reaction mixture was transferred to a Teflon-lined stainless-steel autoclave and was heated at 120^oC for 6 h. The obtained product was collected, washed with deionized water and ethanol, and then dried at 60^oC for overnight, followed by calcination at 350^oC for 2 h to obtain the $MnCo_2O_4$ nanorods.

S1.3. Synthesis of MnCo$_2$O$_4$-MnO$_2$

As-synthesized MCO powders are dispersed in 40 mL $KMnO_4$ solution (10 mmol) and were stirred for ~30 min to obtain a homogeneous mixture. Then the reaction mixture was hydrothermally treated at120^oC for 2 h. The obtained product was then collected, washed with deionized water and ethanol, and then dried at 60^oC for overnight.

S1.4. Synthesis of Porous Carbon

The coconut fibers were extracted from the coconut husk, washed, and dried. Then 2g of coconut fibers are taken in a Teflon-lined autoclave and ~50 mL of concentrated H_2SO_4 was added to it. The mixture was heated at 200^oC for 24 h and then the obtained black product was collected and washed with water until ~pH 7. The precursor was then dried for overnight at ~70^oC. Solid KOH and the precursor (1:1 weight ratio) were grinded and mixed well using a mortar and pestle and then the mixture was calcinated at 850^oC for 3 h in N_2 atmosphere. The obtained product was porous carbon (PC) which was then washed with water till ~pH 7 and dried at ~70^oC for further use.

S1.5. Synthesis of MnCo$_2$O$_4$MnO$_2$-PC nanocomposite

MCO-MnO$_2$-PC nanocomposites were prepared by employing a simple wet-impregnation method. In a round bottom flask, 80 mg of MCO-MnO$_2$ powders and 20 mg PC were dispersed in water and refluxed for 3 h, and then the obtained product was separated from the solvent by centrifugation and then dried at 60°C for 10 h, for further use.

S2. Characterization and Instrumentation. The characterization of the synthesized materials (MnCo$_2$O$_4$, MnCo$_2$O$_4$-MnO$_2$, porous carbon, MCO-MnO$_2$-PC nanocomposite) were carried out by using the following characterization techniques: (i) X-ray diffraction (XRD) patterns were recorded using a powder X-ray diffractometer (Mini Flex II, Rigaku, Japan) with Cu Kα (λ = 0.15405 nm) radiation at a scanning speed of 3 $^{\circ}$ min^{-1}, (ii) Fourier Transform Infrared spectra (FTIR) were recorded using a IR Affinity-1 spectrophotometer (Shimadzu, japan), (iii) Raman spectra were recorded on a Horiba via Raman microscope with a 633 nm laser excitation, (iv) Field emission scanning electron microscopy (FESEM) images of samples were obtained using Quanta 250 FEG (FEI), (v) High-resolution transmission electron microscopy (HRTEM) and selected area electron diffraction (SAED) images were obtained by JEM-2100 (JEOL), 200 kV equipped with LaB$_6$ filament, (vi) Energy dispersive X-ray spectra (EDS) was obtained from X-Max (Oxford Instruments) attached to a JEOL JEM 2100 TEM operated at 200 kV, (vii) XPS measurements were carried out by using a Thermo-Scientific ESCALAB Xi$^+$ spectrometer having a monochromatic Al Kα X-ray source (1486.6 eV) and a spherical energy analyzer that operates in the CAE (constant analyzer energy) mode. (viii) Multiple point BET surface area was determined by a Surface area and porosimetry analyzer (Micromeritics Tristar 3000, USA).

IVIUMSTAT (10V/5A/8MHz) workstation was used to perform the electrochemical studies.

S3. Electrode preparation:

To fabricate the working electrode, first, a viscous paste of 80 wt % active electrode material with 10 wt % poly(vinylidene fluoride) in N-methyl-2-pyrrolidinone and 10 wt % acetylene black was prepared and then this paste was coated on the nickel foam with dimensions (1.5 cm × 1.5 cm) and dried at 80 $^{\circ}$C for 24 h under vacuum to remove the residual solvent. Mass loading on the Ni foam was ~2 mg.

Only one side of the Ni foam was coated in the case of the working electrode for the asymmetric cell.

S4. Fabrication of an asymmetric supercapacitor (ASC) cell.

The voltammetric charges (Q) were calculated based on the following equations:

$$Q = C_{single} \times \Delta V \times m \tag{S1}$$

where m is the mass of the electrode (g), ΔV is the potential window (V), and C_{single} is the specific capacitance (F g^{-1}) of each electrode measured in a three-electrode setup (calculated from cyclic voltammograms at a scan rate of 10 mV s^{-1}).

Considering the charge/mass ratio for both anode and cathode, balancing of charge was carried out by substituting the above equation as:

$$\frac{q+}{q-} = \frac{m+}{m-} = \frac{Csp- \times \Delta V-}{Csp+ \times \Delta V+}$$

(S2)

Where C_{sp-} is the C_S value obtained for the anode material in the potential window ΔV^-, C_{sp+} is the C_S value obtained for the cathode material in the potential window ΔV^+.

S5. Fabrication of the flexible supercapacitor device.

30 mL distilled water was taken in a beaker and heated on a hotplate. 1.6 g KOH was added to the boiling water followed by the addition of 0.42 g $K_4[Fe(CN)_6]$. Then 3.2 g of PVA was added gradually to the reaction mixture and stirred till a thick gel was formed. This gel was then pasted between the positive and negative electrode and allowed to cool and dried at room temperature overnight.

S6. Equations used:

The values of specific capacitance (C_s) for the three-electrode cell and the two-electrode asymmetric cells were calculated by using the following equation:

$$C_s = \frac{i\Delta t}{m\Delta V}$$

(S3)

Where, i represents the charge or discharge current in Ampere (A), Δt is the discharge time in seconds (s), m represents the mass of supercapacitive material in gram (g) and ΔV is the applied potential window.

For the two-electrode asymmetric cell, the energy density (E), the power density (P), and the Coulombic efficiency (η) were determined by using the following equations:

$$E = \frac{C_s \times (\Delta V)^2}{2}$$

(S4)

$$P = \frac{E}{\Delta t}$$

(S5)

$$\eta(\%)=t_d/t_c \times 100$$

(S6)

where, t_d is the discharging time, t_c is the charging time.
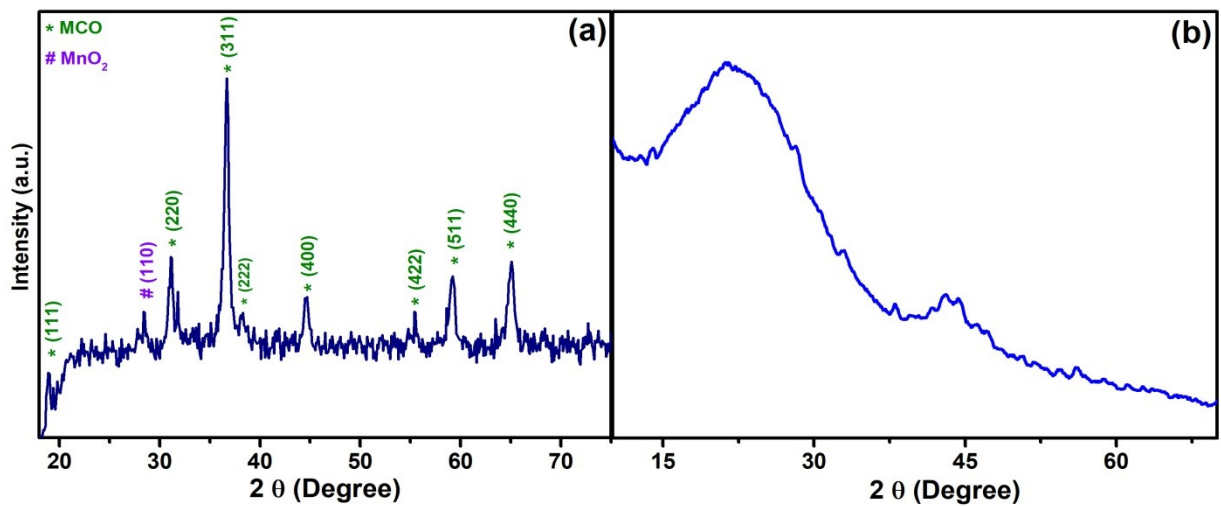
Fig. S1. XRD pattern of (a) MCO-MnO$_2$, (b) porous carbon.
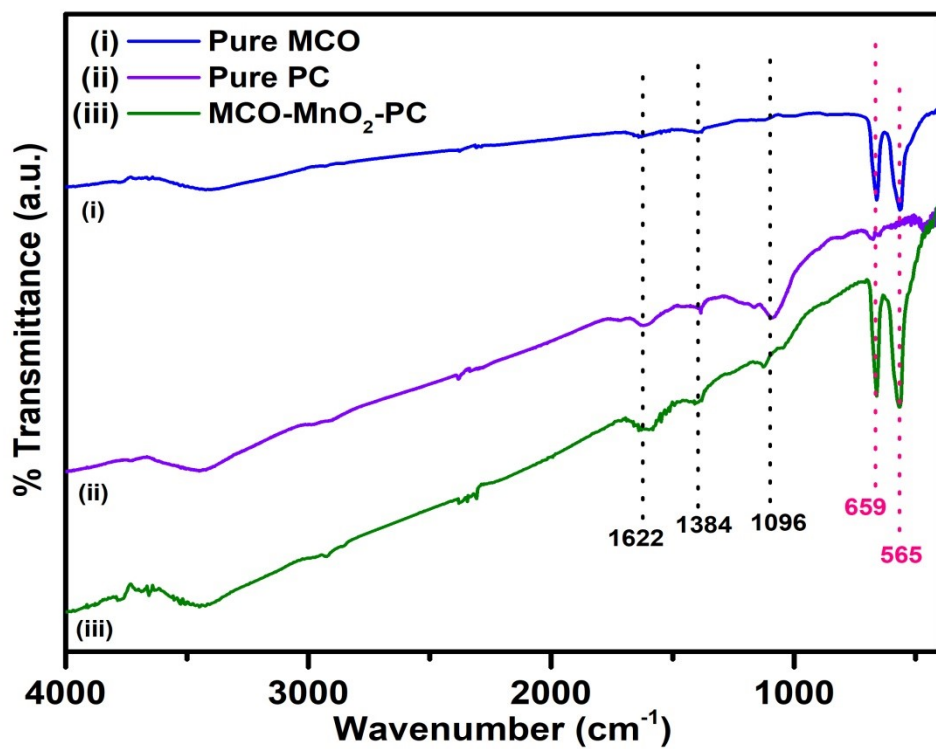
Fig. S2. FT-IR spectra of (i) pure MCO, (ii) pure PC, and (iii) MCO-MnO$_2$-PC nanocomposite.
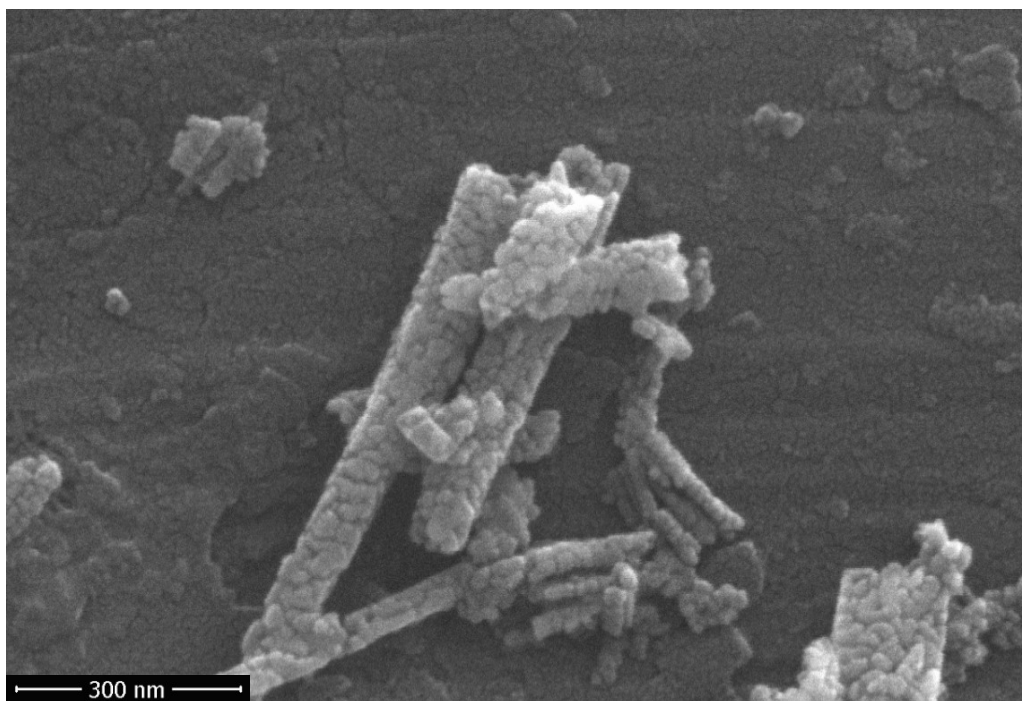
Fig. S3. Magnified FESEM micrograph of pure MCO.
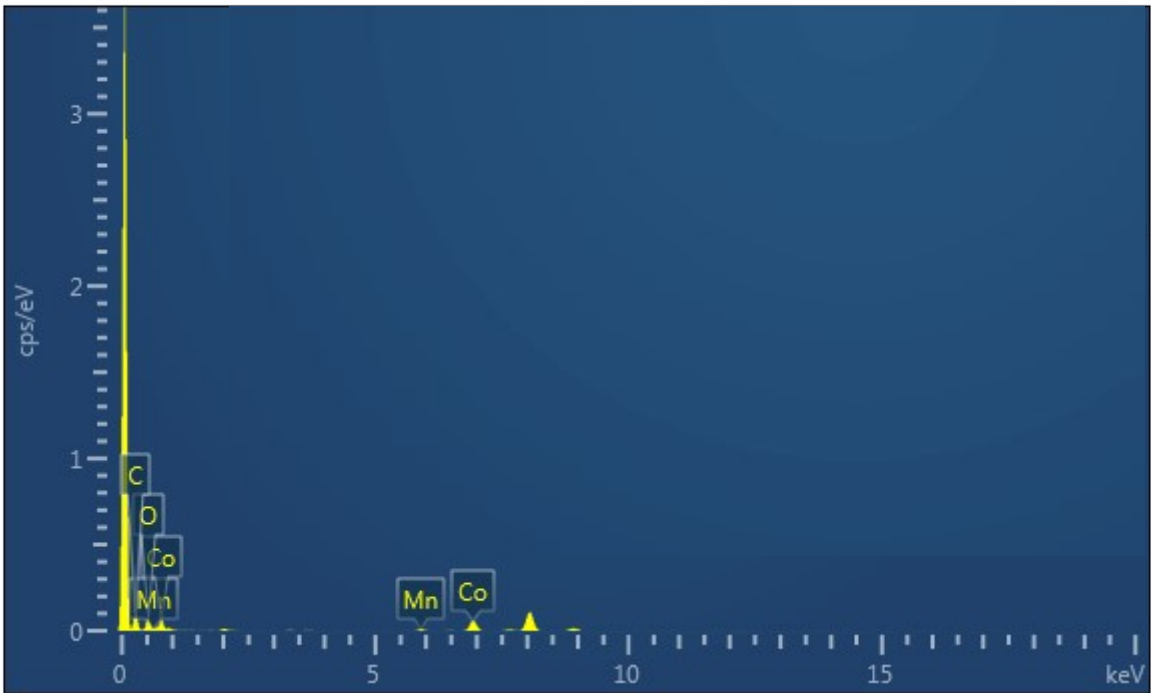
Fig. S4. EDX spectra of MCO-MnO$_2$-PC nanocomposite.
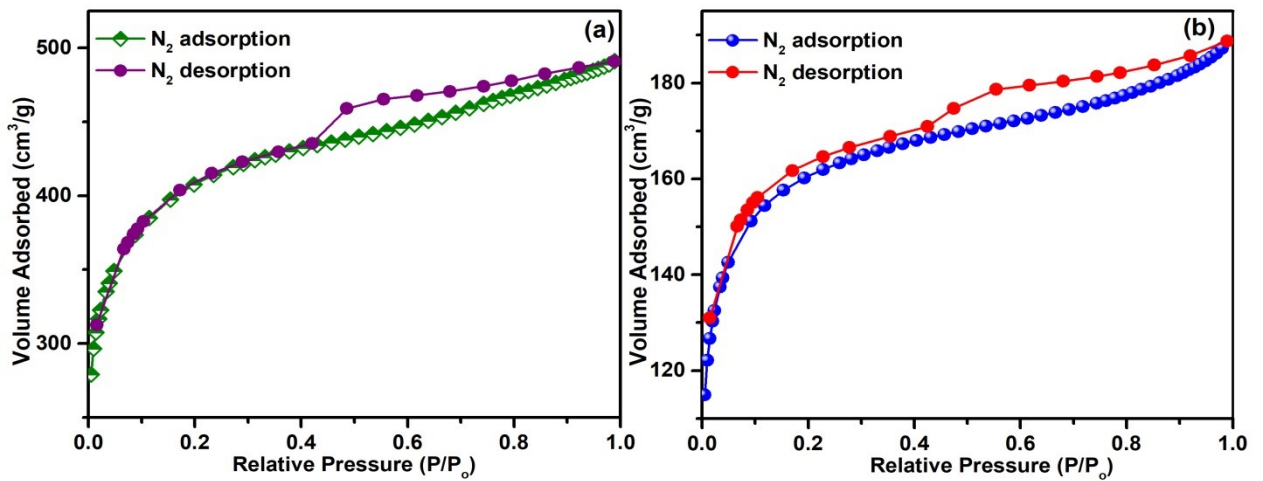
Fig. S5. N$_2$ adsorption and desorption isotherms of (a) PC, and (b) MCO-MnO$_2$-PC.
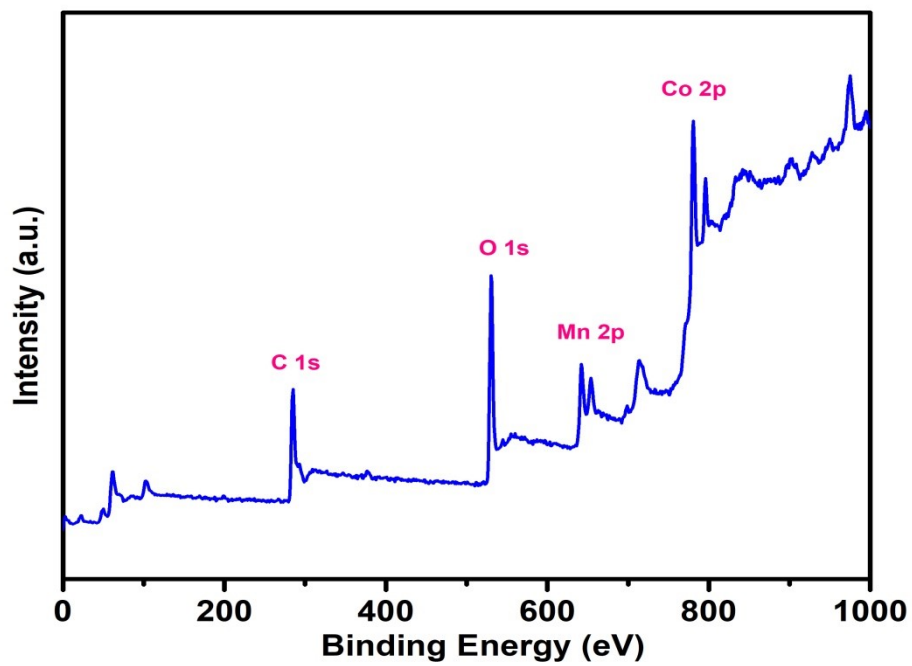
Fig. S6. XPS survey spectrum of MCO-MnO$_2$-PC.
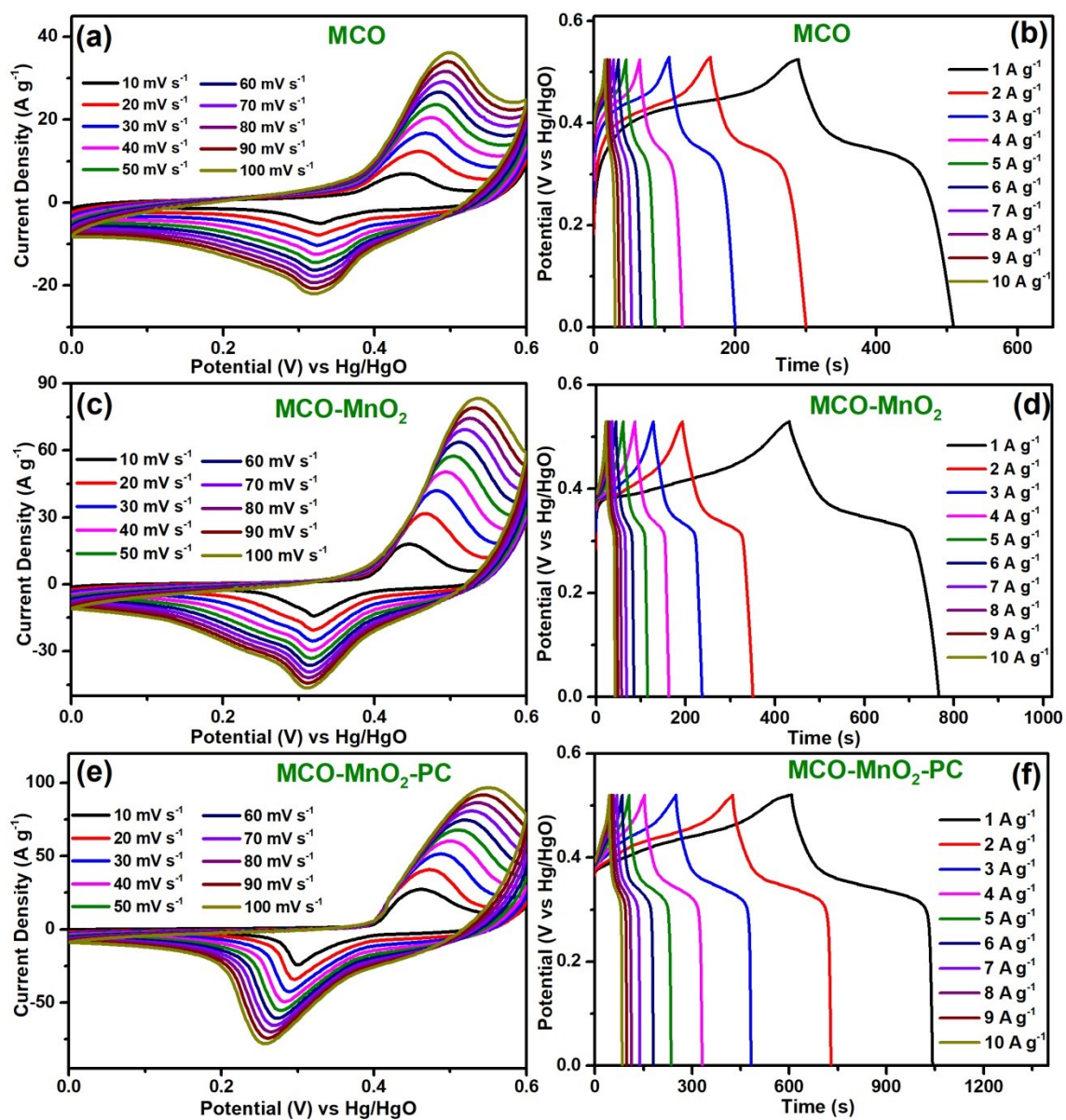
Fig. S7. 3-E cell measurements in 3 M KOH: CV and GCD profiles of (a, b) pure MCO, (c, d) MCO-MnO$_2$, and (e. f) MCO-MnO$_2$-PC nanocomposite.
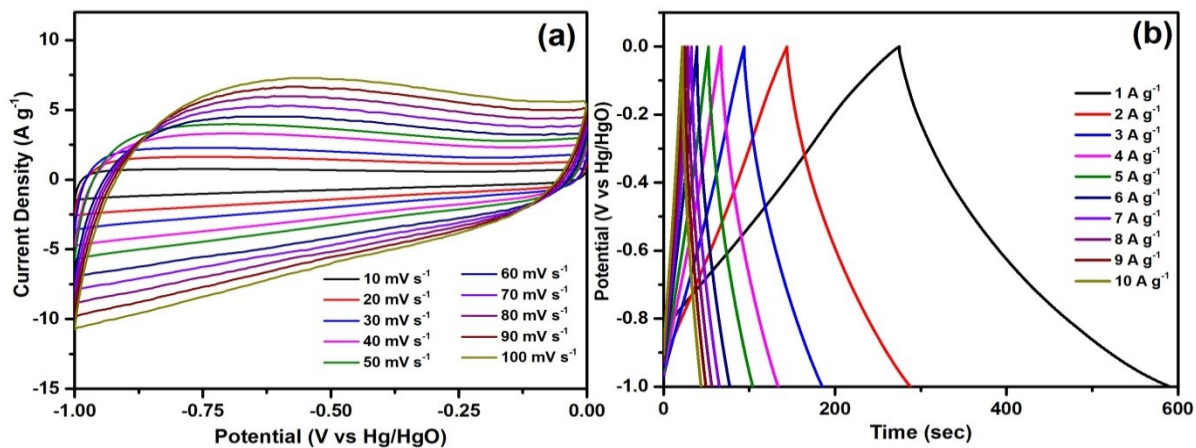
Fig. S8. (a) CV at different scan rates, (b) GCD at different current densities of pure PC in 3 M KOH conducted in a 3-E cell.
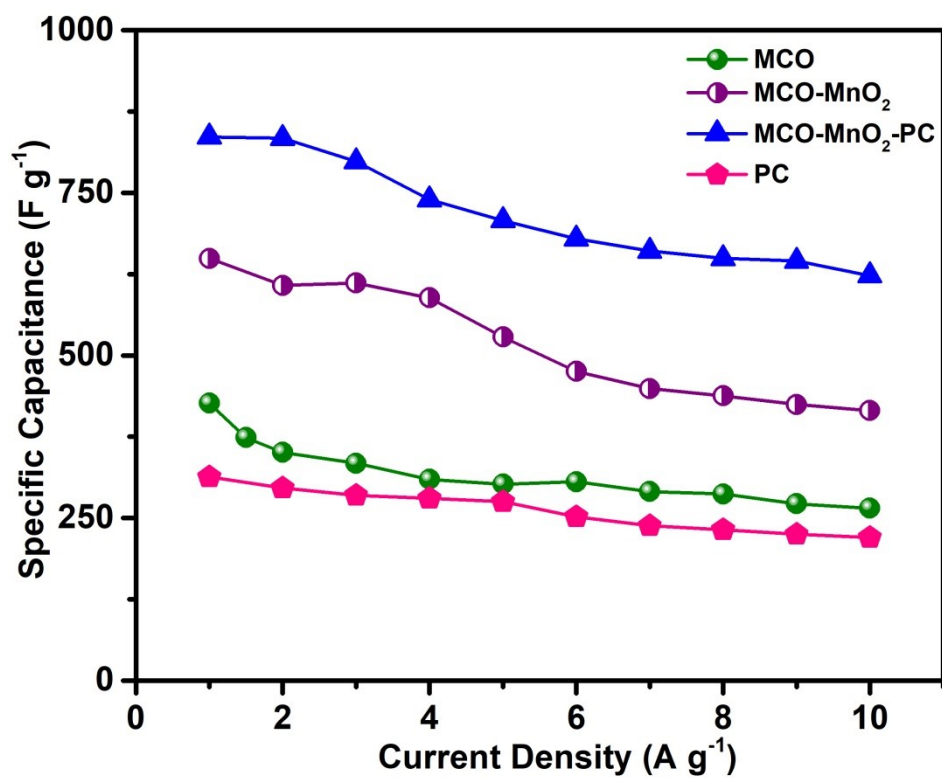
Fig. S9. C_S vs current density plot of the synthesized materials in 3 M KOH.

Table S1. EIS data of all the synthesized materials obtained after circuit fitting.

S. No.	Materials	Equivalent Series Resistance $(R_1=R_S)$ Ω	Charge Transfer Resistance $(R_2=R_{CT})$ Ω	Warburg Resistance (W) Ω	$C_1=C_{DL}$ (F)	$C_2=C_L$ (F)
1	Pure MCO (3 M KOH)	0.94	10.9	1.95E-02	2.55E-03	2.33E-01
2	Pure PC (3 M KOH)	1.11	14.2	7.92E-02	2.75E-03	1.84E-01
3	MCO-MnO$_2$ (3 M KOH)	0.82	2.06	5.45E-03	2.15E-03	3.00E-02
4	MCO-MnO$_2$-PC (3 M KOH)	0.61	1.40	3.31E-03	1.35E-03	5.00E-03
5	MCO-MnO$_2$-PC (0.1 M K$_4$[Fe(CN)$_6$] + 3 M KOH)	0.62	0.56	7.97E-03	1.20E-03	4.46E-03
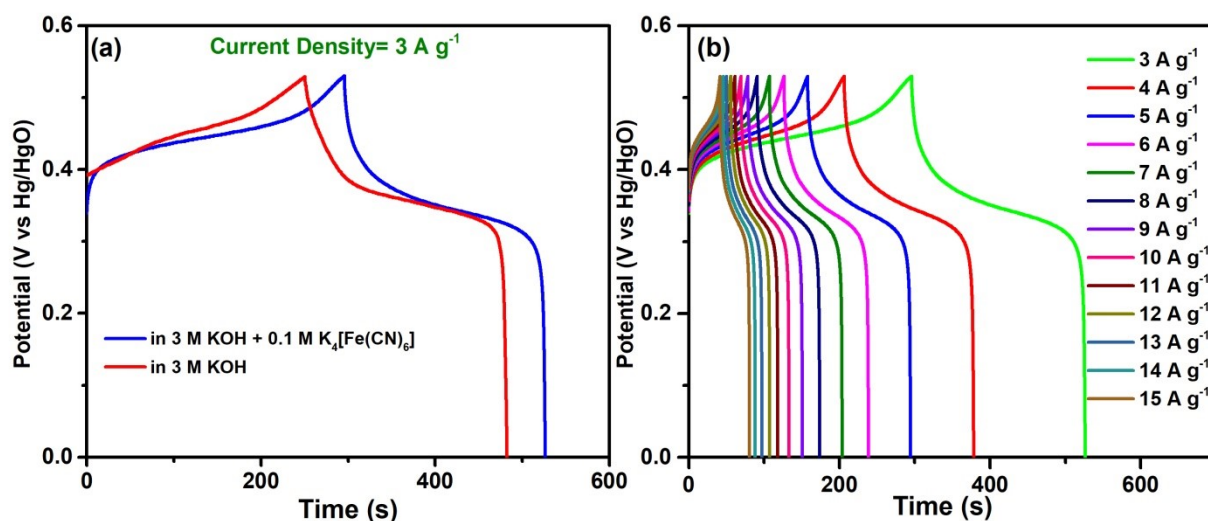
Fig. S10. GCD curve of MCO-MnO$_2$-PC (a) at 3 A g^{-1} in different electrolytes, (b) at different current densities in 3 M KOH + 0.1 M K$_4$[Fe(CN)$_6$] electrolyte system.
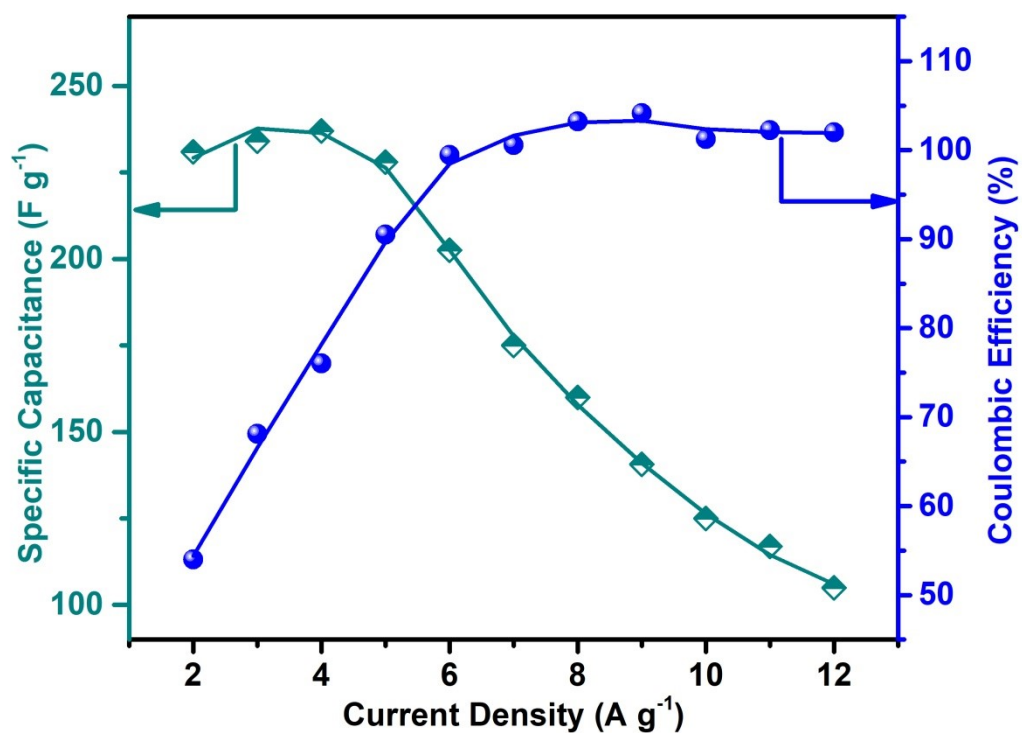
Fig. S11. C_S and Coulombic efficiency of the flexible MCO-MnO$_2$-PC‖PC (all-solid-state) device at increasing current densities.
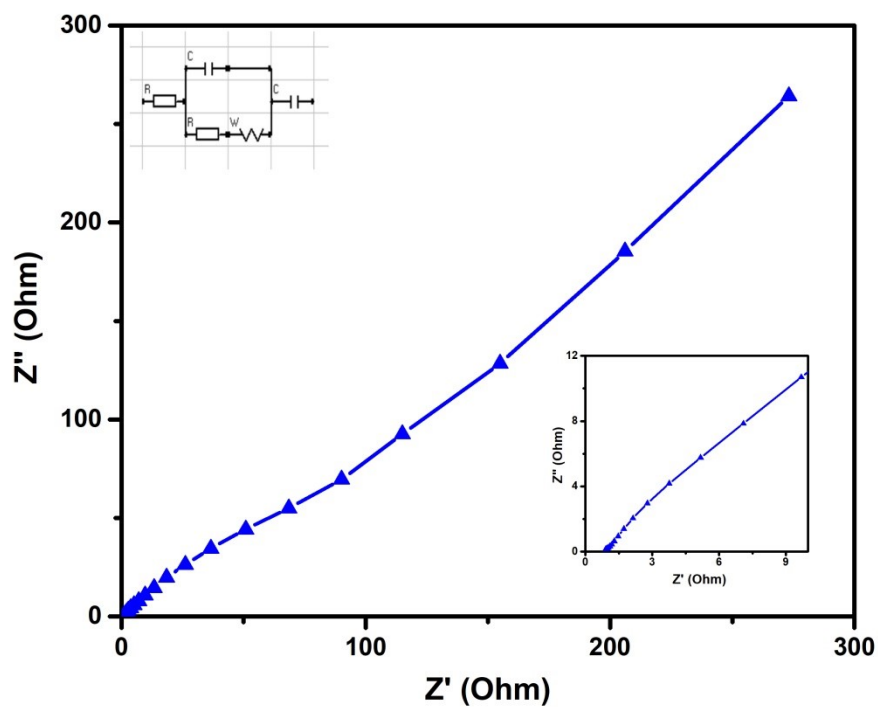
Fig. S12. Nyquist plot of the flexible MCO-MnO$_2$-PC‖PC (all-solid-state) device.
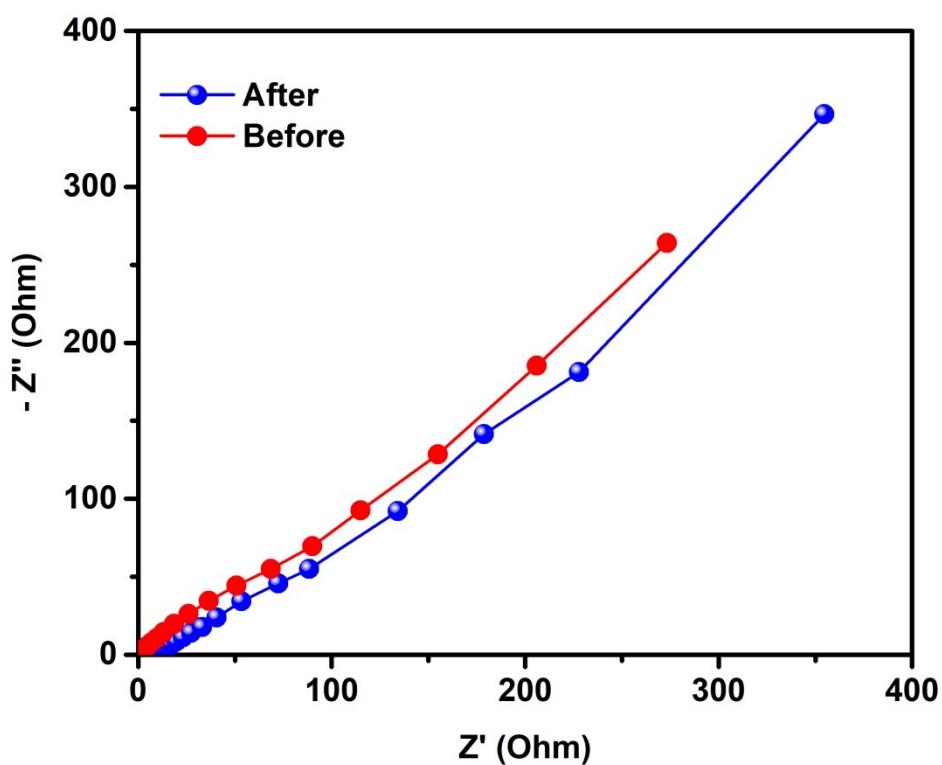
Fig. S13. Nyquist plot of the solid-state MCO-MnO$_2$-PC||PC device before and after ~5000 cycles.
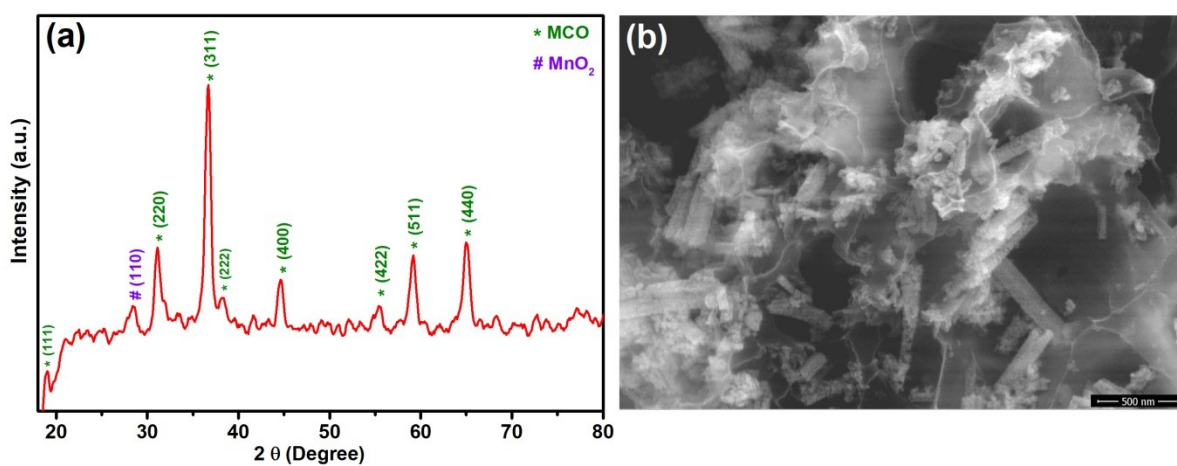
Fig. S14. (a) XRD pattern, (b) FESEM micrograph of MCO-MnO$_2$-PC nanocomposite after ~5000 charge-discharge cycles.

Table S2. Comparison table of the fabricated flexible ASC device (this work) with some of the already reported $MnCo_2O_4$ and carbon-based two-electrode asymmetric supercapacitors.

S. No.	Material	Electrolyte	Working Potential (V)	Power Density (W kg^{-1})	Energy Density (W h kg^{-1})	Retention	Ref.
1.	$MnCo_2O_4$||N-rGO$_{AE}$	1 M KOH	0-1.8	9851.02 (at 4 A g^{-1})	54.11 (at 0.5 A g^{-1})	85.2% (3000 cycles)	1
2.	$MnCo_2O_4$-NG|| NG	2 M KOH	0-1.6	808	48.5	85.9% (10000 cycles)	2
3.	$MnCo_2O_4$@ Ni(OH)$_2$||AC	2 M KOH	0-1.6	1400	48	90% (2500 cycles)	3
4.	PPy@ $MnCo_2O_4$ /GNF||a-MEGO	6 M KOH	0-1.6	16100 (highest)	25.7	85.5% (10000 cycles)	4
5.	$MnCo_2O_4$||rGO	2 M KOH	0-1.6	1600	53.7	82% (5000 cycles)	5
6.	$CoFe_2O_4$||graphene	1 M KOH	0-1.5	643	12.14	67% (3000 cycles)	6
7.	Carbon spheres/MnO_2|| Carbon spheres	0.1 M Na_2SO_4	0-2	100	22.1	99% (1000 cycles)	7
8.	Co_3O_4 NSs-rGO || AC	2 M KOH	0-1.45	2166	13.4	89% (1000 cycles	8
9.	Co_3O_4@CoNiS|| NOPC	3 M KOH	0-1.6	400	46.95	95.6% (20000 cycles)	9
10.	CuO||AC	3 M KOH	0-1.4	700	19.7	96% (3000 cycles)	10
11.	NiS||AC	3 M KOH	0-1.8	900	31	100% (1000 cycles)	11
12.	MnO_2||Graphene hydrogel	0.1 M Na_2SO_4	0-2	1000	23.2	83.4% (5000 cycles)	12
13.	AC||δ-ACEP @MnO_2	1 M Na_2SO_4	0-2	500	31	92.8% (5000 cycles)	13

14.	MnO$_2$/GPCN-SS‖GPCN-SS	1 M Na$_2$SO$_4$	0-2	516	50.2	99.1% (10000 cycles)	[14]
15.	NCS-650‖AC	6 M KOH	0-1.2	331	10.3	88% (5000 cycles)	[15]
16.	NiCoP nanoplates‖graphene films	1 M KOH + Porous polymer membrane (Celgrade 3501)	0-1.5	1301	32.9	83.1 % (5000 cycles)	[16]
17.	CF-200‖LRGONR	PVA/KOH	0-1.6	727.8	33.5	95.8% (5000 cycles)	[17]
18.	L-CoFe$_2$O$_4$/C‖AC	2 M KOH	0-1.6	720	14.38	76.6 (800 cycles)	[18]
19.	CoFe$_2$O$_4$/CNT‖AC	2 M KOH	0-1.6	400	30.4	85.6% (1000 cycles)	[19]
20.	80MnFe$_2$O$_4$-20rGO‖rGO	3 M KOH + 0.1 M K$_4$[Fe(CN)$_6$]	0-1.5	750	27.7	95% (4000 cycles)	[20]
21.	(Ag$_{0.50}$Ni$_{0.50}$)$_{90}$-rGO$_{10}$‖rGO	3 M KOH	0-1.7	1700	49	97% (5000 cycles)	[21]
22.	CuFe$_2$O$_4$-rGO‖rGO	3 M KOH + 0.1 M K$_4$[Fe(CN)$_6$] in PVA	0-1.3	2600	38	97% (10,000 cycles)	[22]
23.	(CoNi$_D$)$_{60}$-rGO$_{40}$‖rGO	3 M KOH + 0.1 M K$_4$[Fe(CN)$_6$] in PVA	0-1.6	2000	52.8	95% (4000 cycles)	[23]
24.	80CF$_{hs}$-20rGO$_{sp}$‖rGO$_{sp}$	3 M KOH + 0.1 M K$_4$[Fe(CN)$_6$] in PVA	0-1.5	1500	65.8	96% (5000 cycles)	[24]

25	60CF-40PC‖PC	3 M KOH + 0.1 M K$_4$[Fe(CN)$_6$] in PVA	0-1.45	1450	50.34	91% (5000 cycles)	[25]
26	MCO-MnO$_2$-PC ‖ PC	3 M KOH + 0.1 M K$_4$[Fe(CN)$_6$] in PVA	0-1.6	1600	81.3	92% (5000 cycles)	**This Work**

References

1. T. Pettong, P. Iamprasertkun, A. Krittayavathananon, P. Sukha, P. Sirisinudomkit, A. Seubsai, M. Chareonpanich, P. Kongkachuichay, J. Limtrakul and M. Sawangphruk, *ACS Appl. Mater. Interfaces*, 2016, **8**, 34045-34053.

2. K. R. Shrestha, S. Kandula, N. H. Kim and J. H. Lee, *J. Alloys Compd.*, 2019, **771**, 810-820.

3. Y. Zhao, L. Hu, S. Zhao and L. Wu, *Adv. Funct. Mater.*, 2016, **26**, 4085-4093.

4. F. Wang, X. Lv, L. Zhang, H. Zhang, Y. Zhu, Z. Hu, Y. Zhang, J. Ji and W. Jiang, *J. Power Sources*, 2018, **393**, 169-176.

5. J. Xu, Y. Sun, M. Lu, L. Wang, J. Zhang, E. Tao, J. Qian and X. Liu, *Acta Mater.*, 2018, **152**, 162-174.

6. K. V. Sankar, R. K. Selvan and D. Meyrick, *RSC Adv.*, 2015, **5**, 99959-99967.

7. Z. Lei, J. Zhang and X. S. Zhao, *J. Mater. Chem.*, 2012, **22**, 153-160.

8. C. Yuan, L. Zhang, L. Hou, G. Pang and W.-C. Oh, *RSC Adv.*, 2014, **4**, 14408-14413.

9. Y. Yan, S. Ding, X. Zhou, Q. Hu, Y. Feng, Q. Zheng, D. Lin and X. Wei, *J. Alloys Compd*, 2021, **867**, 158941.

10. S. E. Moosavifard, M. F. El-Kady, M. S. Rahmanifar, R. B. Kaner and M. F. Mousavi, *ACS Appl. Mater. Interfaces*, 2015, **7**, 4851-4860.

11. B. Guan, Y. Li, B. Yin, K. Liu, D. Wang, H. Zhang and C. Cheng, *Chem. Eng. J.*, 2017, **308**, 1165-1173.

12. H. Gao, F. Xiao, C. B. Ching and H. Duan, *ACS Appl. Mater. Interfaces*, 2012, **4**, 2801-2810.

13. X. Wang, S. Chen, D. Li, S. Sun, Z. Peng, S. Komarneni and D. Yang, *ACS Sustain. Chem. Eng.*, 2018, **6**, 633-641.

14. B. Liu, Y. Liu, H. Chen, M. Yang and H. Li, *ACS Sustain. Chem. Eng.*, 2019, **7**, 3101-3110.

15. F. He, K. Li, S. Cong, H. Yuan, X. Wang, B. Wu, R. Zhang, J. Chu, M. Gong, S. Xiong, Y. Wu and A. Zhou, *ACS Appl. Energy Mater.*, 2021, **4**, 7731-7742.

16. H. Liang, C. Xia, Q. Jiang, A. N. Gandi, U. Schwingenschlögl and H. N. Alshareef, *Nano Energy*, 2017, **35**, 331-340.

17. S. Lalwani, R. B. Marichi, M. Mishra, G. Gupta, G. Singh and R. K. Sharma, *Electrochim. Acta*, 2018, **283**, 708-717.

18. Y. Zhao, Y. Xu, J. Zeng, B. Kong, X. Geng, D. Li, X. Gao, K. Liang, L. Xu and J. Lian, *RSC Adv.*, 2017, **7**, 55513-55522.

19. L. Yue, S. Zhang, H. Zhao, Y. Feng, M. Wang, L. An, X. Zhang and J. Mi, *Solid State Ion.*, 2019, **329**, 15-24.

20. P. Makkar and N. N. Ghosh, *ACS Appl. Energy Mater.*, 2020, **3**, 2653-2664.

21. P. Makkar and N. N. Ghosh, *Ind. Eng. Chem. Res.*, 2021, **60**, 1666-1674.

22. P. Makkar, D. Gogoi, D. Roy and N. N. Ghosh, *ACS Omega*, 2021, **6**, 28718-28728.

23. P. Makkar and N. N. Ghosh, *ACS Omega*, 2020, **5**, 10572-10580.

24. D. Gogoi, M. R. Das and N. N. Ghosh, *ACS Omega*, 2022, 2022, **7**, 11305-11319.

25. D. Gogoi, P. Makkar, M. R. Das and N. N. Ghosh, *ACS Appl. Electron. Mater.*, 2022, **4**, 795-806.